RUSSIAN JOURNAL OF COORDINATION CHEMISTRY, 2025, Vol. 51, No. 1, pp. 3–10

NICKEL(II) COMPLEX WITH THE BIS(PHENOLATE) PINCER N-HETEROCYCLIC CARBENE LIGAND: SYNTHESIS, STRUCTURE, AND PROPERTIES

© 2025 Z. N. Gafurov[a,*], I. K. Mikhailov[a], A. A. Kagilev[a, b], I. F. Sakhapov[a], A. O. Kantyukov[a, b], E. M. Zueva[c], A. B. Dobrynin[a], A. A. Trifonov[d], and D. G. Yakhvarov[b, **]

[a]*A. E. Arbuzov Institute of Organic and Physical Chemistry, Kazan Scientific Center of RAS, Kazan, Russia*

[b]*A. M. Butlerov Chemical Institute, Kazan (Volga Region) Federal University, Kazan, Russia*

[c]*Kazan National Research Technological University, Kazan, Russia*

[d]*A. N. Nesmeyanov Institute of Organoelement Compounds, Russian Academy of Sciences, Moscow, Russia*

**e-mail: gafurov.zufar@iopc.ru*

***e-mail: yakhvar@iopc.ru*

Received August 13, 2024
Revised August 28, 2024
Accepted August 28, 2024

Abstract. The nickel(II) complex Ni(L)Py (I) (L is 1,3-bis(3,5-di-*tert*-butyl-2-phenolato)-5,5-dimethyl-(4,6-dihydropyrimidin-2-ylidene)) containing the dianionic bonded N-heterocyclic carbene (NHC) bis(phenolate) ligand is synthesized. In the presence of a stronger base (4-dimethylaminopyridine (DMAP)), the exchange reaction occurs with the replacement of pyridine in complex I by the DMAP molecule to form complex Ni(L)(DMAP) (II), the crystal structure of which is determined by XRD. The synthesized compounds are characterized by elemental analysis, mass spectrometry, and NMR spectroscopy. The spectral characteristics of the compounds are studied.

Keywords: *nickel(II) complexes, N-heterocyclic carbene ligands, pincer ligands*

DOI: 10.31857/S0132344X250101e3

INTRODUCTION

The growing interest in the chemistry of transition metal complexes with N-heterocyclic carbene (**NHC**) ligands is primarily due to their unique electronic properties, which facilitate the formation of strong $M–C_{NHC}$ bonding, and their chemical behavior [1–8]. These complexes are finding increasing applications in various fields of science, including organic synthesis, materials science and medicine [9–15]. Meanwhile, N-heterocyclic carbene complexes of metals of the nickel subgroup are well established as catalysts for various transformations including cross-coupling, cycloisomerization, polymerization and hydrosilylation reactions [16–25].

For additional tuning of steric and electronic properties of complexes based on N-heterocyclic carbenes, the use of tridentate bisphenolate-NHC ligands of pincer type was previously proposed [2]. According to the HSAB theory [26, 27], the combination of a soft NHC ligand with two hard O-donor anionic groups should significantly affect the electronic structure and functional properties of the metal complexes. Indeed, the high stability, variability and activity of transition metal complexes based on pincer-type ligands have made them indispensable in modern organometallic chemistry and homogeneous catalysis [28–30]. Thus, benzimidazolylidene, imidazolylidene bisphenolate carbene ligands have been used to construct nickel complexes (complexes **A** and **B**, Scheme 1) [2, 31]. The influence of the σ-donating ability of NHC ligands on the catalytic activity and selectivity of reactions catalyzed by transition metal complexes has been reported in a number of works [32–34]. Expansion of the NHC ring has been shown to provide an increase in σ-donor properties [35, 36].

The interest of our research group is directed to the synthesis and catalytic application of pincer complexes of metals of the nickel subgroup [37–43]. The present work describes the synthesis, structure and spectral characterization of an N-heterocyclic carbene bisphenolate nickel complex based on tetrahydropyrimidin-2-ylidene. The N-heterocyclic

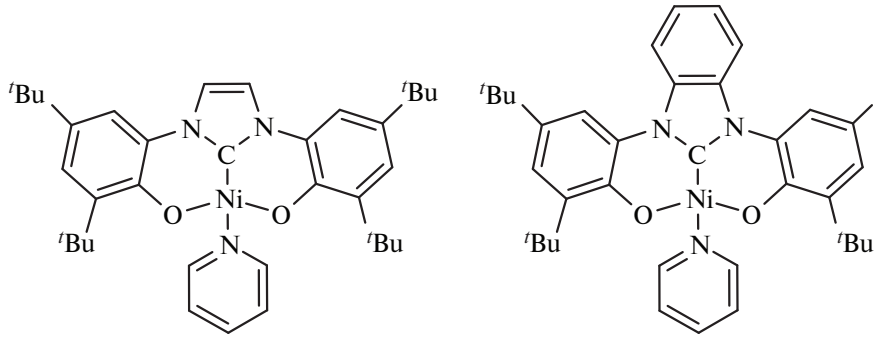

A **B**

Scheme 1.

carbene used is a stronger σ-donor than the ligands of complexes **A** and **B** [44].

EXPERIMENTAL PART

All experiments related to the preparation of initial reagents and electrochemical studies were performed in an inert atmosphere (nitrogen 6.0) using standard Schlenk apparatus. Organic solvents (pentane, dichloromethane, pyridine) were purified and degassed using standard techniques [45]. The starting proligand, 1,3-*bis*(3,5-di-*tert*-butyl-2-hydroxyphenyl)-5,5-dimethyl-3,4,5,6-tetrahydropyrimidin-1-yl chloride (**LH_3Cl**), was prepared according to previously published methods [46]. All other reagents (potassium carbonate (Vecton), anhydrous $NiCl_2$ (Acros), 4-dimethylaminopyridine (DMAP, Acros), and $CDCl_3$ (Solvex)) were used without further purification.

NMR spectra of ^1H, $^{13}C\{^1H\}$ were recorded on a BRUKER AVANCE-400 spectrometer (Germany-Switzerland) at 400.17 MHz (^1H) and 100.62 MHz (^{13}C). The chemical shifts of ^1H and $^{13}C\{^1H\}$ are given relative to tetramethylsilane in ppm and calibrated against the residual proton resonance of the deuterated solvent used. IER mass spectra were taken on a BRUKER AmazonX mass spectrometer (Germany). Detection of positive ions was performed in the *m/z* range from 100 to 2800. The voltage on the capillary is 4500 V. Nitrogen with a temperature of 250°C and a flow rate of 8 l/min was used as a drying gas. The sample was injected at a rate of 4 μl/min using a syringe pump. Elemental analysis was performed on a CHNS high-temperature analyzer Elementar vario MACRO cube (Germany). Absorption spectra of the studied complexes were recorded on a Perkin-Elmer Lambda 35 spectrophotometer (USA) at a sample scanning speed of 480 nm/min with a slit of 1 nm. The spectra of sample solutions in dichloromethane with a concentration of 0.1 mM were recorded in quartz cuvettes 10 mm thick at a temperature of 298 K.

Synthesis of [1,3-*bis*(3,5-di-*tert*-butyl-2-phenolate)-5,5-dimethyl-(4,6-dihydropyrimidin-2-ylidene] pyridine nickel (I). A mixture of LH_3Cl (100 mg, 0.179 mmol), anhydrous $NiCl_2$ (23.2 mg, 0.179 mmol) and potassium carbonate (744 mg, 5.4 mmol, 30 eq.) was suspended using an ultrasonic bath in pyridine (10 mL) in a Schlenk flask. The mixture was then stirred for 12 h at 100°C under nitrogen atmosphere. Thereafter, the volatile components of the resulting suspension were removed vacuo. The residue was dissolved in dichloromethane, the resulting solution was filtered through a silica gel column, then the solvent was removed in vacuo. The yield was complex I (85 mg, 68%, brown solid).

PMR spectrum: (400.17 MHz; 300 K; $CDCl_3$; δ, ppm): 0.90 (s, 18H, $C(CH_3)_3$), 1.21 (s, 6H, $C(CH_3)_2$), 1.33 (s, 18H, $C(CH_3)_3$), 3.54 (s, 4H, CH_2), 6.90 (d, $^4J_{HH}$ = 2.4 Hz, 2H, $CH_{phenoxy}$), 6.99 (d, $^4J_{HH}$ = 2.3 Hz, 2H, $CH_{phenoxy}$), 7.28 (t, $^3J_{HH}$ = 6.3, 2H, CH_{Py}), 7.67 (t, $^3J_{HH}$ = 7.7, 1H, CH_{Py}), 8.86 (d, $^3J_{HH}$ = 5.4, 2H, NCH_{Py}). Spectrum $^{13}C\{^1H\}$ NMR (100.62 MHz; 300 K; $CDCl_3$; δ, ppm): 24.6 ($C(CH_3)_2$), 28.4 ($C(CH_3)_3$), 29.3 ($C(CH_3)_3$), 31.8 ($C(CH_3)_3$), 34.9 ($C(CH_3)_3$), 57.3 (NCH_2), 113.3 (CH_{Ar}), 118.9 (CH_{Ar}), 123.5 (CH_{Py}), 134.5 (*C*–O), 137.2 (CH_{Py}), 137.3 (C_{Ar}), 138.6 (C_{Ar}), 150.5 (CH_{Py}), 154.3 (C_{Ar}), 173.3 ($C_{carbene}$).

IER mass spectrum (in CH_3CN), *m/z*: 576.41 $[I–Py]^+$, 519.51 $[L+H]^+$; 655.36 $[I]^-$.

Found, %: C70.73; H 8.38; N6.33.
For $C_{39}H_{55}N_3O_2Ni$
calculated, %: C71.34; H 8.44; N6.40.

Synthesis of [1,3-*bis*(3,5-di-*tert*-butyl-2-phenolate)-5,5-dimethyl-(4,6-dihydropyrimidin-2-ylidene] (4-dimethylaminopyridine) nickel (II). To a solution of complex I (15 mg, 0.023 mmol) in dichloromethane (2 mL) a solution of 4-dimethylaminopyridine (**DMAP**) (3.4 mg, 0.028 mmol, 1.2 eq.) in dichloromethane (2 mL) was added. The resulting mixture was stirred at room temperature for 2 h, after which all volatile components of the mixture were removed in vacuo, the product was extracted with pentane (3 mL) and filtered through a Schott filter. The filtrate was incubated for

3 days at −10°C, which resulted in the formation of red crystals. The mother liquor was decanted, the crystals were washed with cold pentane and dried in vacuo. The yield of complex **II** was 56% (9 mg, red colored solid). Crystals of complex **II** suitable for X-ray diffraction study were obtained from the solution in pentane by slow evaporation of the solvent.

PMR spectrum: (400.17 MHz; 300 K; $CDCl_3$; δ, ppm): 0.96 (s, 18H, $C(CH_3)_3$), 1.18 (s, 6H, $C(CH_3)_2$), 1.32 (s, 18H, $C(CH_3)_3$), 2.99 (c, 6H, $N(CH_3)_2$) 3.51 (s, 4H, CH_2), 6.40 (d, $^3J_{HH}$ = 6.2 Hz, 2H, CH_{DMAP}), 6.89 (c, 2H, $CH_{phenoxy}$), 6.97 (c, 2H, $CH_{phenoxy}$), 8.29 (d, $^3J_{HH}$ = 6.2 Hz, 2H, CH_{DMAP}). NMR spectrum: $^{13}C\{^1H\}$ (100.62 MHz; 300 K; $CDCl_3$; δ, ppm): 24.1 ($C(CH_3)_2$), 29.2 ($N(CH_3)_2$), 29.9 ($C(CH_3)_3$), 31.6 ($C(CH_3)_3$), 34.5 ($C(CH_3)_3$), 35.4 ($C(CH_3)_3$), 61.7 (NCH_2), 119.9 (*C*HAr), 122.6 (CH_{Ar}), 132.2 (CH_{Py}), 139.5 (*C*–O), 143.0 (C_{Ar}), 148.1 (C_{Ar}), 154.7 (CH_{Py}), 165.4 ($C_{carbene}$).

IER mass spectrum (in CH_3CN), *m/z*: 659.37 [II–DMAP+2CH_3CN]$^+$, 698.36 [II]$^-$

Found, %: C70.52; N8.73; N7.93.
For $C_{41}H_{60}N_4O_2Ni$
calculated, %: C70.39; N8.64; N8.01.

X-ray crystallography of a single crystal of compound **II** was performed on an automatic diffractometer Bruker D8 QUEST (Germany) with MoK_α-radiation (0.71073 Å) at a temperature of 120(2) K. Data acquisition and indexing, determination and refinement of unit cell parameters, absorption correction, accounting for systematic errors, and determination of the crystal space group were performed using the APEX4 software package (v2021.10–0, Bruker AXS). The structure was decoded by the SHELXT-2018/2 software [47] and refined by the full-matrix least-squares method on F^2 by the SHELXL-2018/3 software [48]referred to simply as 'a CIF'. The final refinement was performed by the Olex2 software [49]. All non-hydrogen atoms are refined in the anisotropic approximation. Hydrogen atoms are placed in geometrically calculated positions and included in the refinement in the riding model. The crystallographic data and details of the diffraction experiment are summarized in Table 1.

Crystallographic parameters have been deposited in the Cambridge Structural Data Bank (CCDC No. 2366418; http://www.ccdc.cam.ac.uk)

Quantum-chemical molecular structure calculations were performed by the B3LYP density functional method [50, 51] using the all-electron basis set cc-pVDZ [52, 53] taking into account the influence of dispersion interactions [54, 55] broader range of applicability, and less empiricism. The main new ingredients are atom-pairwise specific dispersion coefficients and cutoff radii that are both computed from first principles. The coefficients for new eighth-order dispersion terms are computed using established recursion relations. System (geometry (computational procedure B3LYP-D3(BJ)/cc-pVDZ). Vertical singlet-singlet electronic transitions (absorption spectra) were calculated by the TD-DFT method within the Tamma-Dankov approximation [56–58]. The basic working equations of TD-DFRT are then derived in a form analogous to the time-dependent Hartree–Fock (TDHF using the B3LYP density functional and the extended def2-TZVP basis set [59–61] (computational procedure TD-B3LYP/def2-TZVP). All quantum chemical calculations were performed using the ORCA 4.0 software package [62].

RESULTS AND DISCUSSION

The precursor N-heterocyclic carbene ligand LH_3Cl was prepared according to the described method [46]. The synthesis of its nickel complex was carried out using a modified procedure proposed earlier for related complexes **A** and **B** [2]. Thus, the interaction of the proligand LH_3Cl with anhydrous nickel dichloride and an excess of potassium carbonate in pyridine at 100°C for 12 h (Scheme 1) led to the formation of complex **I** in 68% yield. The formation of the corresponding bisphenolate N-heterocyclic carbene complex was confirmed by the presence of a carbene carbon atom signal on the NMR spectrum of $_{13}C\{_1H\}$ at 173.3 ppm. At the same time NC(H)N and OH protons of tetrahydropyrimidine and phenol of the initial proligand were not detected when analyzing the ^1H NMR spectra. Note that the values of chemical shifts $\delta_{carbene}$ described for complexes **A** and **B** are much smaller (146.8 ppm for **A** and 162.4 ppm for **B**), which reflects the σ-donor ability of NHC ligands increasing in the series of complexes **A**, **B**, and **I** [36]. A complete assignment of the signals in the ^1H and $^{13}C\{^1H\}$ NMR spectra for complex **I** is presented in the Experimental Part. The proposed formula of the complex was also confirmed by elemental analysis and ESI mass spectrometry.

Despite numerous attempts, a crystal of the complex **I** suitable for X-ray diffraction study could not be obtained. However, it was found that in the presence of a stronger base (DMAP), an exchange reaction occurs with the replacement of pyridine in the complex **I** with a DMAP molecule to form the complex **II** (Scheme 2). In the NMR$^{13}C\{^1H\}$ spectrum of the complex **II**, a singlet with a chemical shift of 165.4 ppm corresponds to the carbene carbon atom (the complete assignment of signals in NMR ^1H and $^{13}C\{^1H\}$ spectra for the complex **II** is presented in the Experimental part). According to X-ray crystallography data, the complex **II** crystallizes in the space group $P2_1/n$. The Ni(1) atom is in a distorted plano-square environment formed by C(1), O(1), O(2) and N(3) atoms (Fig. 1), which is in full agreement with the diamagnetism of the obtained complex. The pyridine occupies a *trans* position relative to the ipso-carbon of the pincer ligand. The Ni–O bond lengths are 1.851(2) and 1.820(3) Å

Table 1. Crystallographic data and parameters of structure refinement complex **II**

Parameter	Value
Gross formula	$C_{41}H_{60}N_4O_2Ni$
M	699.64
Color, habitus	Red-orange, prism
Crystal dimensions, mm	0.311 × 0.205 × 0.177
Shooting temperature, K	120
Syngony	Monoclinic
Sp. group	$P2_1/n$
a, Å	15.1781(8)
b, Å	13.1021(6)
c, Å	24.6441(12)
α, Å	90
β, Å	100.061(2)
γ, Å	90
V, Å^3	4825.5(4)
Z	4
ρ(ded.), g/cm^3	0.963
μ, mm^{-1}	0.433
F(000)	1512
θ_{min}-$\theta_{max,}$ deg	2.94 to 53.992.
Reflection index intervals	$-19 \leqslant h \leqslant 19, -16 \leqslant k \leqslant 16, -31 \leqslant l \leqslant 31$
Reflections measured	94542
Independent reflections	10535 (R_{int} = 0.0758, R_{sigma} = 0.0355)
Reflections with $I > 2\sigma(I)$	10535
Reflections/restrictions/parameters	10535/139/499
GOOF	1.228

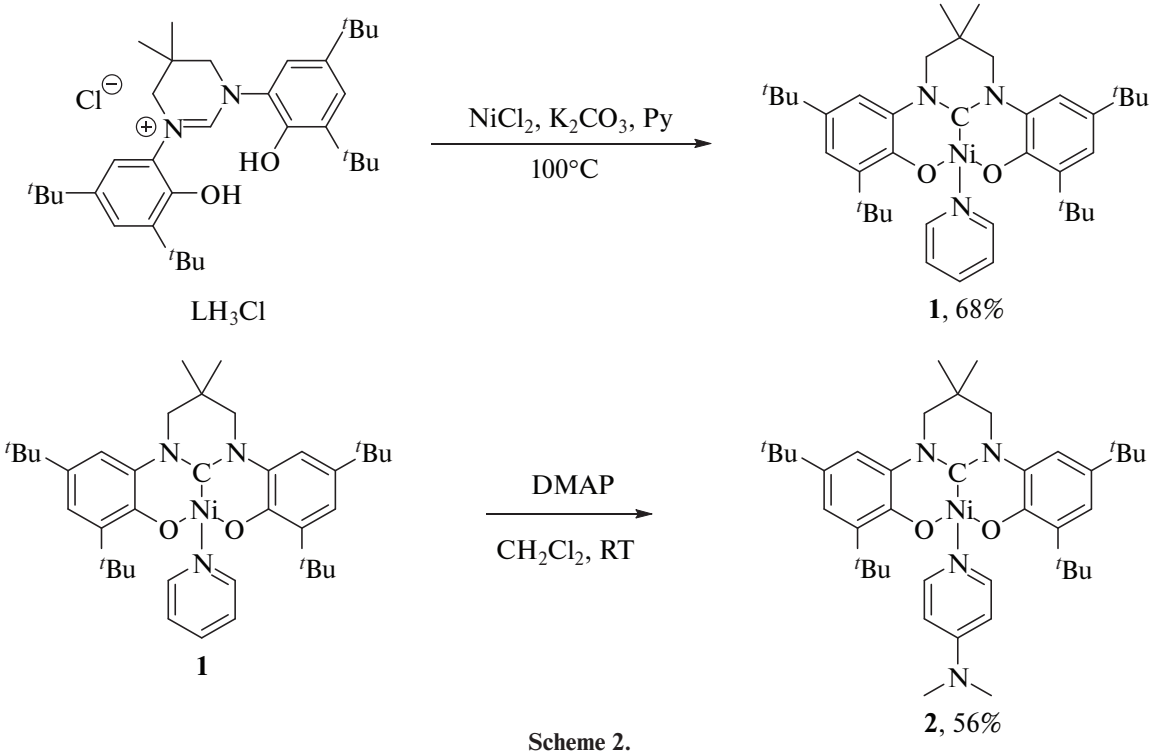

Scheme 2.

and agree well with the Ni–$O_{Phenoxy}$ distances in the analogous phenolate complex A (1.847(2) and 1.835(2) Å). At the same time, the Ni–$C_{carbene}$ bond length (1.851(4) Å) is longer than in the case of complex A (1.794(3) Å). Also worth noting is the significant deviation from the OCONi plane of the |O(1)–N(1)–N(2)–O(2)| = 44.33° fragment (29.97° for A) [2].

Fig. 2 shows the optimized structure of the complex **I**. Selected bond lengths (Å) and angles (deg) for the complexes **I**, **II**, and **A** are given in Table 2. Quantum chemical calculations of the molecular structure predict a deviation of the NHC fragment from the plane defined by OCO atoms, which is in agreement with the results of the diffraction analysis carried out for the complex **II**. The Ni–$C_{carbene}$ bond length (1.876 Å) in the optimized structure of the complex **I** is also longer than that found for its analog **A**.

According to Fig. 3 (red line), the absorption maxima of 0.1 mM solution of the complex **I** in dichloromethane are detected at wavelengths of 311 nm (ε = 9580 $M^{-1} \times cm^{-1}$) and 382 nm (ε = 2600 M^{-1} × cm^{-1}). According to quantum chemical calculations, both absorption bands correspond to intraligand π–π* (phenolate → NHC) excitations mixed with metal-to-metal charge transfer. Thus, calculations predict a band at 382 nm (f_{osc} = 0.13), for which HOMO → LUMO+2 (47%) and HOMO → LUMO+3 (34%) excitations are responsible, as well as high-energy bands at 339 (f_{osc} = 0.11) and 323 (f_{osc} = 0.08) nm corresponding to HOMO-1 → LUMO+2 (62%) and HOMO-1 → LUMO+3 (75%) transitions, respectively. The absorption spectrum for the complex **II** (Fig. 3, blue line) is almost identical to the spectrum obtained for the complex **I**. It is worth noting that the absorption maximum for the complex **A** is observed at 374 nm and for the complex **B** at 393 nm [31]; these bands are similarly assigned to phenolate → NHC transitions.

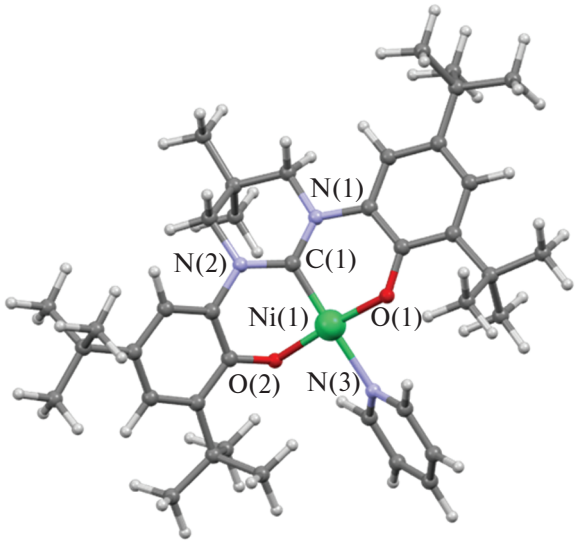

Fig. 2. Structure of the complex **I** optimized as a result of quantum chemical calculation by density functional theory (B3LYP-D3(BJ)/cc-pVDZ).

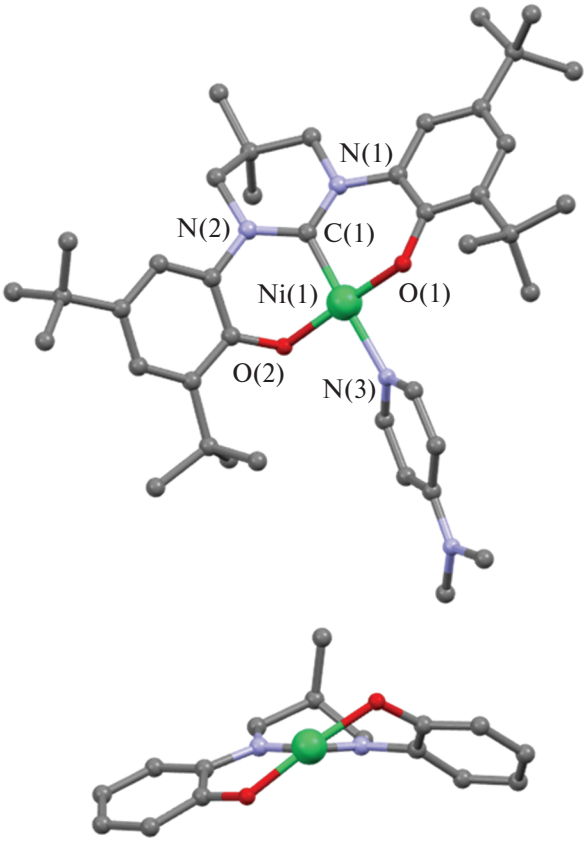

Fig. 1. Molecular structure of the complex **II** (top) and C–Ni axis view (bottom; *t*-Bu groups and DMAP not shown). Selected bond lengths and angles: C(1)–Ni(1), 1.851(4); N(3)–Ni(1), 1.972(3); O(1)–Ni(1), 1.851(2); O(2)–Ni(1), 1.820(3) Å; N(1) C(1) N(2) 117.9(3)°; C(1) Ni(1) O(2) 91.6(1)°; C(1) Ni(1) O(1) 91.8(1)°; O(2) Ni(1) O(1) 173.9(1)°; C(1) Ni(1) N(3) 174.1(1)°.

Thus, in the present work, the pyridine complex of nickel **I** with pincer tetrahydropyrimidine-2-ylidene O, C, O-bisphenolate ligand was synthesized and isolated in good yield. The interaction of the complex **I** with DMAP leads to the substitution of pyridine in the complex **I** with DMAP molecule to form the complex **II**, the structure of which in the crystal was unambiguously established by X-ray crystallography and confirmed by NMR spectroscopy in solution. The nickel atom in the complex is characterized by a flat-quadratic ligand environment, which is in full agreement with the diamagnetism of the obtained complex. The reversal of the NHC fragment of the pincer ligand relative to the plane defined by [OCONi] atoms is 44.33°, which is much larger than that found for the similar nickel A complex based on imidazol-2-ylidene (29.97°). Quantum chemical

Table 2. Comparison of the selected bond lengths (Å) and angles (deg) in **I**, **II**, and **A***

Complex	Ni(1)–O(1)	Ni(1)–O(2)	Ni(1)–C(1)	|O(1)–N(1)–N(2)–O(2)|
I (calculated)	1.879	1.838	1.876	41.48
II (exp.)	1.851(2)	1.820(3)	1.851(4)	44.33
A (exp.) [2]	1.847(2)	1.835(2)	1.794(3)	29.97

*Experimental values were obtained from X-ray crystal structures; Calculated values were obtained from quantum chemical calculation (B3LYP-D3(BJ)/cc-pVDZ).

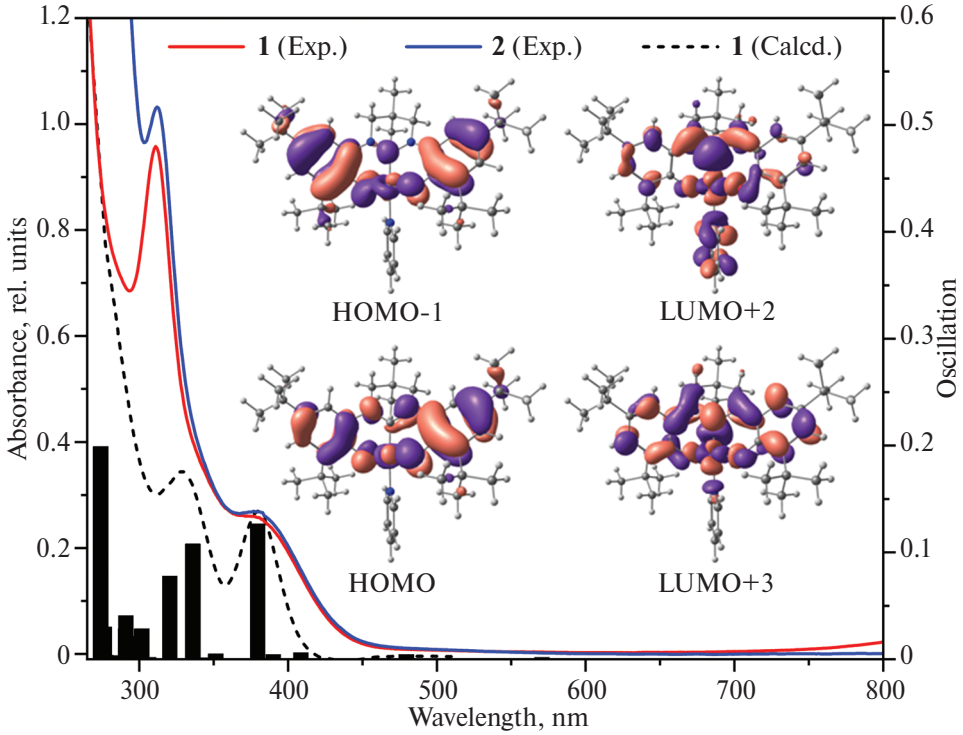

Fig. 3. Absorption spectra of 0.1 mM solutions of the complexes I (red line) and II (blue line) in dichloromethane at 298 K. The dotted line represents the calculated absorption spectrum (TD-B3LYP/def2-TZVP) for the complex I (red line) and II (blue line). The vertical bars represent the calculated electronic transitions for the complex I. Inset: molecular orbitals of the complex I participating in electronic transitions (contour value 0.03).

calculation of the molecular structure of the complex **I** predicts an elongation of the Ni–$C_{carbene}$ bond compared to A, which is consistent with the X-ray crystallography data for **II**.

CONFLICT OF INTEREST

The authors declare that they have no conflict of interest.

ACKNOWLEDGEMENTS

Diffraction, mass spectrometric studies and elemental analysis were carried out on the equipment of the Collective Spectro-Analytical Center for Physico-Chemical Studies of the Structure, Properties and Composition of Substances and Materials of the Kazan Scientific Center of Russian Academy of Sciences.

FUNDING

The work on the synthesis of nickel carbene complexes described in this work was performed within the framework of the State Assignment of the Federal Research Center, Kazan Scientific Center RAS. The spectral studies by nuclear magnetic resonance method were carried out at the expense of the subsidy provided to Kazan Federal University for the fulfillment of the State Assignment in the field of scientific activity (No. FZSM-2023-0020)

REFERENCES

1. *Lapshin I.V., Cherkasov A.V., Lyssenko K.A. et al.* // Inorg. Chem. 2022. V. 61. No. 24. P. 9147. https://doi.org/10.1021/acs.inorgchem.2c00698
2. *Borré E., Dahm G., Aliprandi A. et al.* // Organometallics. 2014. V. 33. No. 17. P. 4374. https://doi.org/10.1021/om5003446
3. *Fosu E., Le N., Abdulraheem T. et al.* // Organometallics 2024. V. 43. No. 4. P. 467. https://doi.org/10.1021/acs.organomet.3c00411
4. *Sheng H., Liu Q., Su X. – D. et al.* // Org. Lett. 2020. V. 22. No. 18. P. 7187. https://doi.org/10.1021/acs.orglett.0c02523
5. *Li J., Wang L., Zhao Z. et al.* // Angew. Chemie Int. Ed. 2020. V. 59. No. 21. P. 8210. https://doi.org/10.1002/anie.201916379
6. *Rao J., Dong S., Yang C. et al.* // J. Am. Chem. Soc. 2023. V. 145. No. 47. P. 25766. https://doi.org/10.1021/jacs.3c09280
7. *Karaaslan M.G., Aktaş A., G□rses C. et al.* // Bioorg. Chem. 2020. V. 95. P. 103552. https://doi.org/10.1016/j.bioorg.2019.103552
8. *Gafurov Z.N., Kantyukov A.O., Kagilev A.A. et al.* // Russ. Chem. Bull. 2017. V. 66. No. 9. P. 1529. https://doi.org/10.1007/s11172–017–1920–7
9. *Zhao Q., Meng G., Nolan S.P. et al.* // Chem. Rev. 2020. V. 120. No. 4. P. 1981. https://doi.org/10.1021/acs.chemrev.9b00634
10. *Sau S.C., Hota P.K., Mandal S.K. et al.* // Chem. Soc. Rev. 2020. V. 49. No. 4. P. 1233. https://doi.org/10.1039/c9cs00866g
11. *Zhao Q., Han B., Peng C. et al.* // Med. Res. Rev. 2024. https://doi.org/10.1002/med.22039
12. *Bellotti P., Koy M., Hopkinson M.N. et al.* // Nat. Rev. Chem. 2021. V. 5. No. 10. P. 711. https://doi.org/10.1038/s41570–021–00321–1
13. *Ibáñez S.*, *Poyatos M.*, *Peris E.* // Acc. Chem. Res. 2020. V. 53. No. 7. P. 1401. https://doi.org/10.1021/acs.accounts.0c00312
14. *Ott I.* // Adv. Inorg. Chem. 2020. V. 75. P. 121. https://doi.org/10.1016/bs.adioch.2019.10.008
15. *Liang Q.*, *Song D.* // Chem. Soc. Rev. 2020. V. 49. No. 4. P. 1209. https://doi.org/10.1039/c9cs00508k
16. *Strausser S.L.*, *Jenkins D.M.* // Organometallics. 2021. V. 40. No. 11. P. 1706. https://doi.org/10.1021/acs.organomet.1c00189
17. *Kashina M.V., Luzyanin K.V., Katlenok E.A. et al.* // Dalton Trans. 2022. V. 51. No. 17. P. 6718. https://doi.org/10.1039/d2dt00252c
18. *Zhan L., Zhu M., Liu L. et al.* // Inorg. Chem. 2021. V. 60. No. 21. P. 16035. https://doi.org/10.1021/acs.inorgchem.1c01964
19. *Bernd M.A., Bauer E.B., Oberkofler J. et al.* // Dalton Trans. 2020. V. 49. No. 40. P. 14106. https://doi.org/10.1039/d0dt02598d
20. *Sánchez A., Sanz-Garrido J., Carrasco C.J. et al.* // Inorg. Chim. Acta. 2022. V. 537. P. 120946. https://doi.org/10.1016/j.ica.2022.120946
21. *Li M., Liska T., Swetz A. et al.* // Organometallics. 2020. V. 39. No. 10. P. 1667. https://doi.org/10.1021/acs.organomet.0c00065
22. *Rendón-Nava D., Angeles-Beltrán D., Rheingold A.L. et al.* // Organometallics. 2021. V. 40. No. 13. P. 2166. https://doi.org/10.1021/acs.organomet.1c00324
23. *Rivera C., Bacilio-Beltrán H.A., Puebla-Pérez A.M. et al.* // New J. Chem. Chem. 2022. V. 46. No. 29. P. 14221. https://doi.org/10.1039/d2nj02508f
24. *Neshat A.*, *Mastrorilli P.*, *Mobarakeh A.M.* // Molecules. 2022. V. 27. No. 1. P. 95. https://doi.org/10.3390/molecules27010095
25. *Díez-González S.*, *Marion N.*, *Nolan S.P.* // Chem. Rev. 2009. V. 109. No. 8. P. 3612. https://doi.org/10.1021/cr900074m
26. *Pearson R.G.* // Inorg. Chem. 1973. V. 12. No. 3. P. 712. https://doi.org/10.1021/ic50121a052
27. *Pearson R.G.* // Inorg. Chem. 1988. V. 27. No. 4. P. 734. https://doi.org/10.1021/ic00277a030
28. *Gunanathan C.*, *Milstein D.* // Chem. Rev. 2014. V. 114. No. 24. P. 12024. https://doi.org/10.1021/cr5002782
29. *Maser L.*, *Vondung L.*, *Langer R.* // Polyhedron. 2018. V. 143. P. 28. https://doi.org/10.1016/j.poly.2017.09.009
30. *Taakili R.*, *Canac Y.* // Molecules. 2020. V. 25. No. 9. P. 2231. https://doi.org/10.3390/molecules25092231
31. *Gandara C., Philouze C., Jarjayes O. et al.* // Inorg. Chim. Acta. 2018. V. 482. P. 561. https://doi.org/10.1016/j.ica.2018.06.046
32. *Nolan S.P.* // N-Heterocyclic Carbenes Eff. Tools Organomet. Synth. 2014. V. 9783527334. P. 1. https://doi.org/10.1002/9783527671229
33. *Dröge T.*, *Glorius F.* // Angew. Chem. Int. Ed. 2010. V. 49. No. 39. P. 6940. https://doi.org/10.1002/anie.201001865
34. *Wittwer B., Leitner D., Neururer F.R. et al.* // Polyhedron. 2024. V. 250. P. 116786. https://doi.org/10.1016/j.poly.2023.116786
35. *Chesnokov G.A., Topchiy M.A., Dzhevakov P.B. et al.* // Dalton Trans. 2017. V. 46. No. 13. P. 4331. https://doi.org/10.1039/c6dt04484k
36. *Meng G., Kakalis L., Nolan S.P. et al.* // Tetrahedron Lett. 2019. V. 60. No. 4. P. 378. https://doi.org/10.1016/j.tetlet.2018.12.059
37. *Luconi L., Gafurov Z., Rossin A. et al.* // Inorg. Chim. Acta. 2018. V. 470. P. 100. https://doi.org/10.1016/j.ica.2017.03.026
38. *Luconi L., Garino C., Cerreia Vioglio P. et al.* // ACS Omega. 2019. V. 4. No. 1. P. 1118. https://doi.org/10.1021/acsomega.8b02452

39. *Luconi L., Tuci G., Gafurov Z.N. et al.* // Inorg. Chim. Acta. 2020. V. 517. P. 120182. https://doi.org/10.1016/j.ica.2020.120182

40. *Gafurov Z.N., Kantyukov A.O., Kagilev A.A. et al.* // Russ. J. Electrochem. 2021. V. 57. No. 2. P. 134. https://doi.org/10.1134/S1023193521020075

41. *Gafurov Z.N., Kagilev A.A., Kantyukov A.O. et al.* // Russ. Chem. Bull. 2018. V. 67. No. 3. P. 385. https://doi.org/10.1007/s11172–018–2086–7

42. *Gafurov Z.N., Bekmukhamedov G.E., Kagilev A.A. et al.* // J. Organomet. Organomet. Chem. 2020. V. 912. P. 121163. https://doi.org/10.1016/j.jorganchem.2020.121163

43. *Kagilev A.A., Gafurov Z.N., Sakhapov I.F. et al.* // J. Electroanal. Electroanal. Chem. 2024. V. 956. P. 118084. https://doi.org/10.1016/j.jelechem.2024.118084

44. *Gurina G.A., Markin A.V., Cherkasov A.V. et al.* // Eur. J. Inorg. Chem. 2023. V. 26. No. 29. P. E202300392. https://doi.org/10.1002/ejic.202300392

45. *Armarego W.L.F.* Purification of Laboratory Chemicals. Amsterdam: Butterworth-Heinemann, 2017.

46. *Long J., Lyubov D.M., Gurina G.A. et al.* // Inorg. Chem. 2022. V. 61. No. 3. P. 1264. https://doi.org/10.1021/acs.inorgchem.1c03429

47. *Sheldrick G.M.* // Acta Crystallogr. A. 2015. V. 71. No. 1. P. 3. https://doi.org/10.1107/S2053273314026370

48. *Sheldrick G.M.* // Acta Crystallogr. C. 2015. V. 71. P. 3. https://doi.org/10.1107/S2053229614024218

49. *Dolomanov O.V., Bourhis L.J., Gildea R.J. et al.* // J. Appl. Appl. Crystallogr. 2009. V. 42. No. 2. P. 339. https://doi.org/10.1107/S0021889808042726

50. *Becke A.D.* // J. Chem. Phys. 1993. V. 98. No. 7. P. 5648. https://doi.org/10.1063/1.464913

51. *Stephens P.J., Devlin F.J., Chabalowski C.F. et al.* // J. Phys. Phys. Chem. 1994. V. 98. No. 45. P. 11623. https://doi.org/10.1021/j100096a001

52. *Dunning T.H.* // J. Chem. Phys. 1989. V. 90. No. 2. P. 1007. https://doi.org/10.1063/1.456153

53. *Woon D.E.*, *Dunning T.H.* // J. Chem. Chem. Phys. 1993. V. 98. No. 2. P. 1358. https://doi.org/10.1063/1.464303

54. *Grimme S., Antony J., Ehrlich S. et al.* // J. *Chem*. Chem. Phys. 2010. V. 132. No. 15. P. 154104. https://doi.org/10.1063/1.3382344

55. *Grimme S.*, *Ehrlich S.*, *Goerigk L.* // J. Comput. Comput. Chem. 2011. V. 32. No. 7. P. 1456. https://doi.org/10.1002/jcc.21759

56. *Casida M.E.* // Recent Advances in Computational Chemistry. 1995. V. 1. Pt. 1. P. 155. https://doi.org/10.1142/9789812830586_0005

57. *Adamo C.*, *Jacquemin D.* // Chem. Soc. Rev. 2013. V. 42. No. 3. P. 845. https://doi.org/10.1039/c2cs35394f

58. *Laurent A.D.*, *Adamo C.*, *Jacquemin D.* // Phys. Chem. Chem. Phys. 2014. V. 16. No. 28. P. 14334. https://doi.org/10.1039/c3cp55336a

59. *Weigend F.*, *Ahlrichs R.* // Phys. Chem. Chem. Phys. 2005. V. 7. No. 18. P. 3297. https://doi.org/10.1039/b508541a

60. *Weigend F.* // Phys. Chem. Chem. Phys. 2006. V. 8. No. 9. P. 1057. https://doi.org/10.1039/b515623h

61. *Peterson K.A., Figgen D., Goll E. et al.* // J. Chem. Chem. Phys. 2003. V. 119. No. 21. P. 11113. https://doi.org/10.1063/1.1622924

62. *Neese F.* // Wiley Interdiscip. Rev. Comput. Mol. Sci. 2018. V. 8. No. 1. P. E1327. https://doi.org/10.1002/wcms.1327